

# Recording from two neurons: second order stimulus reconstruction from spike trains and population coding

N. M. Fernandes, B. D. L. Pinto, L. O. B. Almeida, J. F. W. Slaets and R. Köberle

*Depart. de Física e Informática, Inst. de Física de São Carlos, USP, C. P. 369, CEP 13560-970, São Carlos-SP, Brasil, e-mail: rk@if.sc.usp.br*

October 16, 2018

We study the reconstruction of visual stimuli from spike trains, recording simultaneously from the two H1 neurons located in the lobula plate of the fly *Chrysomya megacephala*. The fly views two types of stimuli, corresponding to rotational and translational displacements. If the reconstructed stimulus is to be represented by a Volterra series and correlations between spikes are to be taken into account, first order expansions are insufficient and we have to go to second order, at least. In this case higher order correlation functions have to be manipulated, whose size may become prohibitively large. We therefore develop a Gaussian-like representation for fourth order correlation functions, which works exceedingly well in the case of the fly. The reconstructions using this Gaussian-like representation are very similar to the reconstructions using the experimental correlation functions. The overall contribution to rotational stimulus reconstruction of the second order kernels - measured by a chi-squared averaged over the whole experiment - is only about 8% of the first order contribution. Yet if we introduce an instant-dependent chi-square to measure the contribution of second order kernels at special events, we observe an up to 100% improvement. As may be expected, for translational stimuli the reconstructions are rather poor. The Gaussian-like representation could be a valuable aid in population coding with large number of neurons.

# 1 Introduction

---

Living animals have to reconstruct a representation of the external world from the output of their sensory systems in order to correctly react to the demands of a rapidly varying environment. In many cases this sensory output is encoded into a sequence of identical action potentials, called spikes. If we represent the external world by a time-dependent stimulus function  $s(t)$ , the animal has to reconstruct  $s(t)$  from a set of spikes. This decoding procedure generates an estimate  $s_e(t)$  of the stimulus like a digital-to-analog converter.

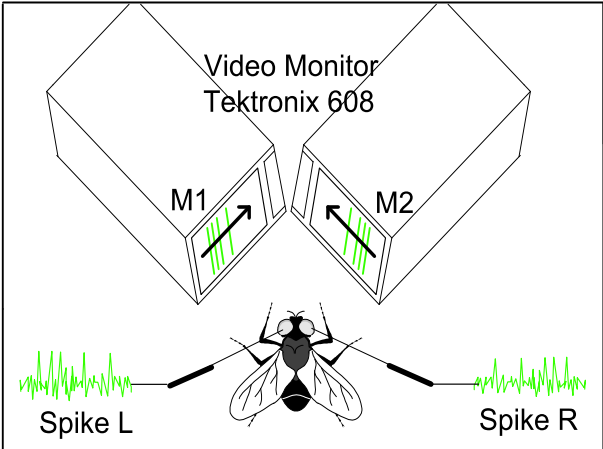


Figure 1: Motion sensitivity of the two H1 neurons. Each eye sees a monitor displaying a rigidly moving bar pattern. The stimuli in this figure correspond to a translational motion in which both neurons are excited. Inverting the stimulus shown by monitor M1 would generate a rotational stimulus, which now inhibits the response of the left neuron. Electrodes record extracellularly from each H1.

Here we study this decoding procedure in a prominent example of spiking neurons: the two H1 neurons of the fly *Chrysomya megacephala*. The fly has two compound eyes with their associated neural processing systems (Hausen, 1981, 1982, 1984). Motion detection starts at the photoreceptor cells, eight of them located in each one of the  $\sim 5000$  ommatidia of each compound eye. They effect the transduction of photons into electrical signals, which are propagated via the lamina and medulla to the lobula plate. This neuropil is - inter alia - composed of horizontally and vertically directionally sensitive wide field neurons. The H1 neurons are horizontally sensitive and are excited by ipsilateral back to front motion and inhibited by oppositely moving stimuli.

## Rotational and Translational Rasters

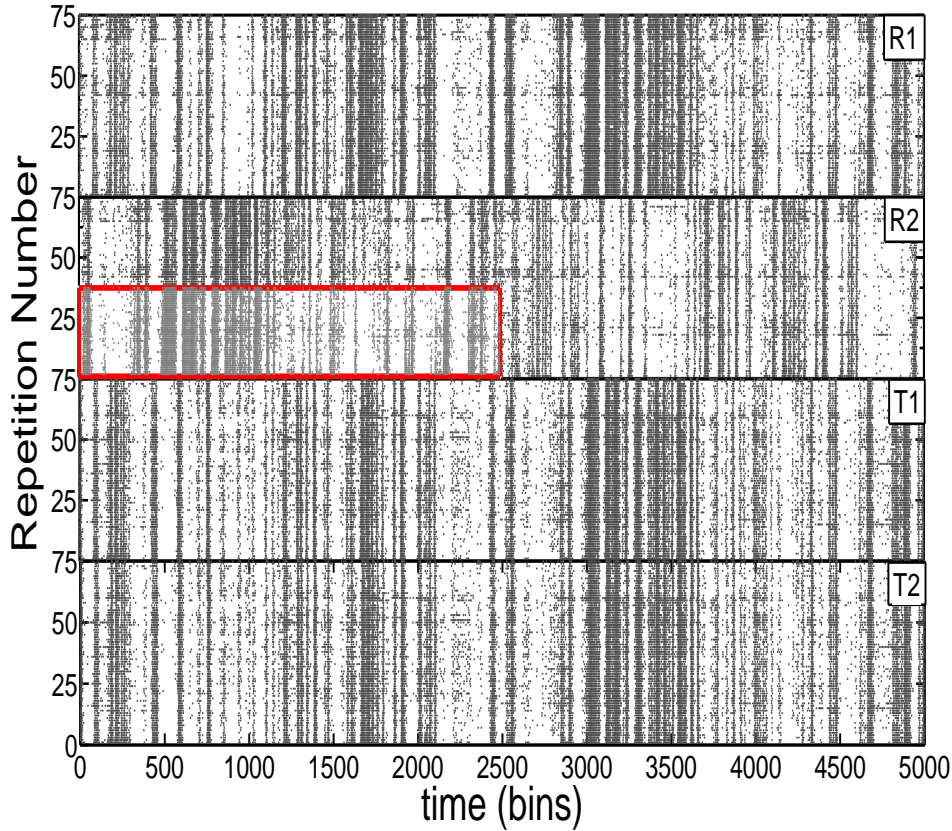


Figure 2: Raster plot for the two H1 neurons, showing their complementary action under rotational and translational stimuli. The same time-dependent stimulus  $s(t)$  is repeatedly shown to the fly, the horizontal time axis running from time zero to 5000 bins = 10 seconds and the vertical axis showing the repetition number. The responses of the neurons are shown as a raster, where each dot represents a spike. The right H1 sees a stimulus  $s_r(t)$  and the left one sees  $s_l(t)$ . Rotational stimuli  $s_r(t) = s_l(t) = s(t)$ : (R1) spikes from right H1 and (R2) spikes from left H1. Translational stimuli  $s_r(t) = -s_l(t) = s(t)$ : (T1) spikes from right H1 and (T2) spikes from left H1. Inset to (R2): Spikes from right H1, fly subjected to sign reversed stimuli in order to simulate raster (R2).

Each H1 neuron projects its axon to the contralateral lobula plate, exciting there two horizontal and two centrifugal cells. These cells mediate mutual

inhibition between the two H1 neurons (Haag, Vermeulen, & Borst, 1999; Haag & Borst, 2001; Farrow, Haag, & Borst, 2003; Haag & Borst, 2008; Krapp, 2009)<sup>1</sup>. We subject the fly to rotational and translational stimuli - see Figure 1. If the fly rotates around a vertical axis, say clockwise when looking down the axis, the left neuron is inhibited and the right one is excited, so that the two neurons become an efficient rotational detector (Hausen, 1984). This can be seen in Figure 2 (R1) & (R2). Even when recording only from the ipsilateral H1, one can simulate the response of the contralateral H1. In fact, since the two H1 cells have mirror symmetric directional sensitivities, the sign flipped stimulus induces a response in the ipsilateral H1 typical for the contralateral H1 cell (Rieke, Warland, Steveninck, & Bialek, 1997). The inset in (R2) shows this to be true to a very good approximation.

In forward translation none of H1 neurons is excited, corresponding to the low spike density regions in the raster-plots of Figure 2 (T1) & (T2). In backward translation, both H1's are excited and we expect a strong inhibition. Yet the spike rate is comparable to rotational excitation - compare Figure 2 (R1) & (T1). Numerical computation confirms this visual impression. Nevertheless in translation the two H1's fire mainly in sync, which leads to subtle differences with respect to rotation. As a consequence, our reconstructions will be much poorer for the translational case - see section 5.

If we want to take correlations between spikes into account, instead of treating them independently, we have to go at least to second order stimulus reconstructions. These require the computation of higher order spike-spike correlation functions and a subsequent matrix inversion. If one records from many neurons simultaneously, the size of these matrices may soon become prohibitively large. Here we present an efficient representation of these higher order correlation functions in terms of second order ones. The reconstruction now costs far less computationally, avoids large matrix inversions and gives excellent results. We test the quality of our reconstructions under both rotational and translational stimuli.

If this representation holds more generally, it may well make population coding computationally more tractable. We briefly discuss a perturbation scheme, which allows a stepwise inclusion of small effects.

---

<sup>1</sup>Although experimental work has focussed on the vertical system, one expects analog results for the horizontal one.

## 2 Stimulus reconstruction from spike trains .

Suppose we want to reconstruct the stimulus from the response of a single H1 neuron. We represent this response as a spike train  $\rho(t) = \sum_{i=1}^{N_s} \delta(t - t_i)$ , which is a sum of delta functions at the spike times  $t_i$ .  $N_s$  is the total number of spikes generated by the neuron during the experiment.

The simplest reconstruction extracts the stimulus estimate via a linear transformation, see e.g. (Rieke et al., 1997; Bialek, Rieke, Steveninck, & Warland, 1991),

$$s_e(t) = \int_{-\infty}^{\infty} k_1(\tau) \rho(t - \tau) d\tau, \quad (2.1)$$

with the kernel  $k_1(t)$  to be determined.

For simplicity we effect an *acausal* reconstruction, i.e. we integrate from  $-\infty$  to  $+\infty$ . Essentially the same results are obtained in a causal reconstruction. One way to implement causality proceeds to estimate the stimulus at time  $t$ , using as input the spike train up to time  $t + t_0$ . For the fly  $t_0$  has to be  $\gtrsim$  to 30 milliseconds. In this case equation 2.1 would read:  $s_e(t) = \int_{-t_0}^{\infty} k_1(\tau) \rho(t - \tau) d\tau$ .

Equation 2.1 is the first term of a Volterra series (Martin, 2006):

$$s_e(t) = \int_{-\infty}^{\infty} k_1(\tau) \rho(t - \tau) d\tau + \int_{-\infty}^{\infty} k_2(\tau_1, \tau_2) \rho(t - \tau_1) \rho(t - \tau_2) d\tau_1 d\tau_2 + \dots \quad (2.2)$$

There is no convergence proof for this expansion, but heuristically we may say that it should be a valid approximation, if the average number of spikes per correlation time  $\tau_c$ ,

$$\eta = \langle r \rangle \tau_c, \quad (2.3)$$

is small (Rieke et al., 1997). Here  $\langle r \rangle$  is the mean spike rate and  $\tau_c$  a typical signal correlation time. For small  $\eta$  each spike gives independent information about the stimulus. In our case  $\eta \sim 0.6 - 0.8$ , which is of the order of unity, so that higher order effects might be relevant.

The first order term, being proportional to  $\sum_i^{N_s} k_1(t - i_i)$ , independently adds contributions for each spike. Yet it is well established that pairs of spikes carry a significant amount of additional information beyond the single spike contributions (Brenner, Strong, Köberle, Bialek, & Steveninck, 2000). This motivates the addition of the second order kernel  $k_2(\tau_1, \tau_2)$ , which includes correlations between up to two spikes.

In order to obtain the kernels  $k_1$  and  $k_2$  we choose to minimize the following functional - the  $\chi^{(2)}$  error -

$$\chi^{(2)}(k_1, k_2) = \langle \int dt [s_e(t) - s(t)]^2 \rangle. \quad (2.4)$$

The brackets stand for an ensemble average with respect to the distribution of all possible stimuli in a given experiment. In a long experiment we average over  $N_w \sim 10^5$  time windows of size  $T_w$ . Typically  $T_w \sim 100$  milliseconds - see section 7 for details. For ease of presentation, in the following our discussions will always refer to the rotational setup, unless explicitly stated otherwise as in section 5.

Since the functional 2.4 is quadratic, the equations minimizing  $\chi^{(2)}(k_1, k_2)$

$$\partial\chi^{(2)}/\partial k_j = 0, j = 1, 2 \quad (2.5)$$

are linear in the unknowns  $k_1, k_2$ . E.g., if we keep only  $k_1$ , using therefore equation 2.1, we get:

$$\tilde{k}_1(\omega) = \frac{\langle \tilde{s}(\omega) \star \tilde{\rho}(\omega) \rangle}{\langle \tilde{\rho}(\omega) \star \tilde{\rho}(\omega) \rangle}, \quad (2.6)$$

where Fourier transforms are defined as  $\tilde{F}(\omega) = \int dt F(t)e^{i\omega t}$ .

We may include the second order term  $k_2$ , either as a correction to the first order reconstruction  $s_1(t) = k_1 \star \rho(t)$ <sup>2</sup>, or one may solve the coupled system 2.5.

If we record simultaneously from left and right H1, we obtain two spike trains  $\rho_1(t)$  and  $\rho_2(t)$ . The expansion equation 2.2 generalizes to

$$s_e(t) = K_1 \star \rho_1(t) + K_2 \star \rho_2(t) + K_{11} \star \rho_1 \star \rho_1(t) + K_{12} \star \rho_1 \star \rho_2(t) + K_{22} \star \rho_2 \star \rho_2(t) + \dots \quad (2.7)$$

Here we have included the kernel  $K_{12}$ , which encodes effects correlating  $\rho_1$  and  $\rho_2$ <sup>3</sup>. Notice that  $K_{12} = K_{21}$ .

To first order, keeping only  $K_1$  and  $K_2$  in the expansion 2.7, we get the following equations:

$$\tilde{\mathcal{R}}_a(\omega) = \sum_{b=1}^2 \tilde{K}_b(\omega) \tilde{R}_{ab}(\omega), \quad a = 1, 2 \quad (2.8)$$

---

<sup>2</sup>The symbol  $\star$  stands for a convolution as in equation 2.1.

<sup>3</sup>Notice that we have not *orthogonalized* our expansion equation 2.2, so that there are  $K_{11}(t_1, t_1)$  terms, which could have been absorbed in  $K_1(t)$  and similarly for  $K_2(t)$ .

where

$$\widetilde{\mathcal{R}}_a(\omega) = \int dt dt' \langle s(t') \rho_a(t' - t) \rangle e^{i\omega t}. \quad (2.9)$$

and

$$R_{ab}(t_1, t_2) = \int dt \langle \rho_a(t - t_1) \rho_b(t - t_2) \rangle, \quad a, b = 1, 2. \quad (2.10)$$

Due to time-translation invariance  $R_{ab}(t_1, t_2)$  is only a function of the difference:  $R_{ab}(t_1, t_2) = R_{ab}(t_1 - t_2)$  and  $\widetilde{R}_{ab}(\omega) = \int dt R_{ab}(t) e^{i\omega t}$ . Analogous properties hold for all the following correlation functions involving only  $\rho(t)$ .

The solution of equations 2.8 yields

$$\widetilde{K}_a(\omega) = (L_a(\omega) R_{\hat{a}\hat{a}} - L_{\hat{a}}(\omega) R_{a\hat{a}}(\omega)) / \Delta, \quad a = 1, 2 \quad (2.11)$$

where

$$L_a(\omega) = \langle s(\omega) \rho_a^*(\omega) \rangle, \quad \Delta = R_{11} R_{22} - R_{12} R_{21} \quad (2.12)$$

and  $\hat{a} = 3 - a$ . We obtain the first order reconstruction as

$$s_1(t) = K_1 \star \rho_1(t) + K_2 \star \rho_2(t). \quad (2.13)$$

Since the second order contribution turns out to be small, we treat it as a perturbation to the first order reconstruction. We therefore expand  $s_2(t) = s(t) - s_1(t)$  as:

$$s_2(t) = K_{11} \star \rho_1 \star \rho_1(t) + K_{12} \star \rho_1 \star \rho_2(t) + K_{22} \star \rho_2 \star \rho_2(t). \quad (2.14)$$

We now have to solve the following equations

$$\mathcal{R}_{ab}^{(2)}(t_1, t_2) = \int dt_3 dt_4 \sum_{c,d=1}^2 K_{cd}(t_1, t_2) R_{abcd}^{(4)}(t_1, t_2, t_3, t_4), \quad (2.15)$$

where

$$\mathcal{R}_{ab}^{(2)}(t_1, t_2) = \int dt \langle s_2(t) \rho_a(t - t_1) \rho_b(t - t_2) \rangle, \quad (2.16)$$

$$R_{abcd}^{(4)}(t_1, t_2, t_3, t_4) = \int dt \langle \rho_a(t - t_1) \rho_b(t - t_2) \rho_c(t - t_3) \rho_d(t - t_4) \rangle. \quad (2.17)$$

Although the system 2.15 is linear, the matrices to be inverted may be very large. We have to invert the matrix

$$\mathcal{M}_{AT}^{BT'} \equiv R_{abcd}^{(4)}(t_1, t_2, t_3, t_4), \quad (2.18)$$

where  $A, B$  are compound indices  $A = [ab], B = [cd]$  labeling the neurons.  $T = [t_1, t_2], T' = [t_3, t_4]$  are compound time indices of size  $T_w^2$  each. If we compute the correlation functions using a time window of  $T_w = 128$  bins, with binsize = 2 milliseconds, then the size of  $\mathcal{M}_{AN}^{BN'}$  is  $\sim 128^4 \times 2^4 \sim 5 \times 10^9$ . The matrices to be inverted may become prohibitively large, especially if we record from more than just two neurons<sup>4</sup>.

We therefore present below a Gaussian-like representation of  $R_{abcd}^{(4)}$  with a small number of parameters and which requires no large matrix inversion.

### 3 Gaussian-like (G1) representation for 4-point functions

---

In this section we present a representation of the 4-point function  $R_{abcd}^{(4)}$  in terms of the 2-point function  $R_{ab}^{(2)}$ , which is surprisingly good and which avoids the computation of the large matrices 2.18.

If our spike-generating process were Gaussian, we would have the following structure for  $R^{(4)}$ :

$$R^{(4)}(1, 2, 3, 4) = R(1, 2)R(3, 4) + R(1, 3)R(2, 4) + R(1, 4)R(2, 3) - 2\langle\rho(t)\rangle^4, \quad (3.19)$$

where  $\langle\rho(t)\rangle$  is just a constant, due to time-translation invariance<sup>5</sup>.

This suggests the following representation for  $R^{(4)}$ :

$$R^{(4)}(1, 2, 3, 4) = A [R(1, 2)R(3, 4) + R(1, 3)R(2, 4) + R(1, 4)R(2, 3)] - B, \quad (3.20)$$

where  $A$  and  $B$  are constants to be adjusted<sup>6</sup>.

For two neurons we get the representation:

$$R_{abcd}(1, 2, 3, 4) = [R_{ab}(1, 2)R_{cd}(3, 4) + R_{ac}(1, 3)R_{bd}(2, 4) + R_{ad}(1, 4)R_{bc}(2, 3)]A_{abcd} + B_{abcd} \quad (3.21)$$

---

<sup>4</sup>We may solve the above system in Fourier space and select a subset of frequencies in order to reduce the size of the system.

<sup>5</sup>We write  $(1, 2, \dots)$  instead of  $(t_1, t_2, \dots)$ .

<sup>6</sup>Any structure built only from  $R(t_1, t_2)$  could be used for our method to work.

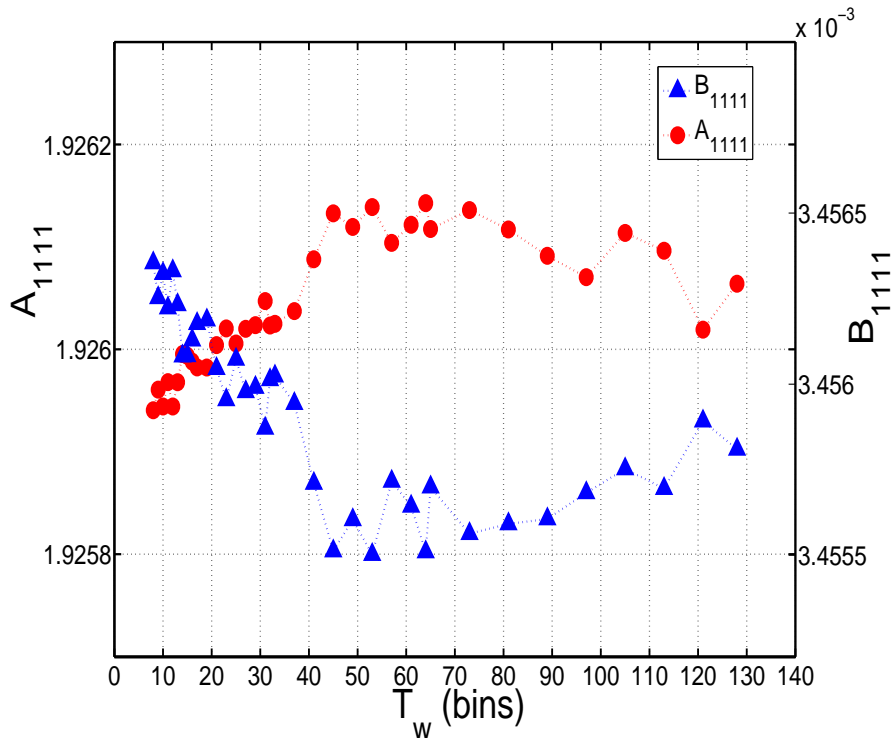


Figure 3: Window-size dependence of parameters  $A_{1111}$  and  $B_{1111}$ . Similar behavior is found for the other parameters  $A$  and  $B$ . Notice that variations are on the 0.05% level.

with  $a, b, c, d = 1, 2$  and  $A_{abcd}, B_{abcd}$  constants to be determined.

The usefulness of our GI-representation scheme depends on the quality of the 4-point functions obtained, which in turn hinges on the knowledge of the constants  $A_{abcd}$  and  $B_{abcd}$ . There would be no point, if this required the computation of 4-point functions in large window sizes and a fitting procedure using these windows - exactly what we wanted to avoid. We therefore fit the constants  $A_{abcd}$  and  $B_{abcd}$  for a sequence of window sizes  $T_w$ , ranging from 10 to 128 bins, using  $R_{1111}(t_1, t_2 = t_3 = t_4 = 1)$  to fit to the experimental data. As can be seen in Figure 3, at least in the fly's case, the dependence of the parameters  $A_{abcd}, B_{abcd}$  on  $T_w$  is only 0.05% and therefore completely negligible. The constants  $A_{abcd}$  and  $B_{abcd}$  can therefore be computed very fast in small windows. In Figure 4 we plot the fits to the first row  $R_{1111}(t_1, t_2 = t_3 = t_4 = 1)$  and its GI approximation. As advertised we obtain a perfect fit.

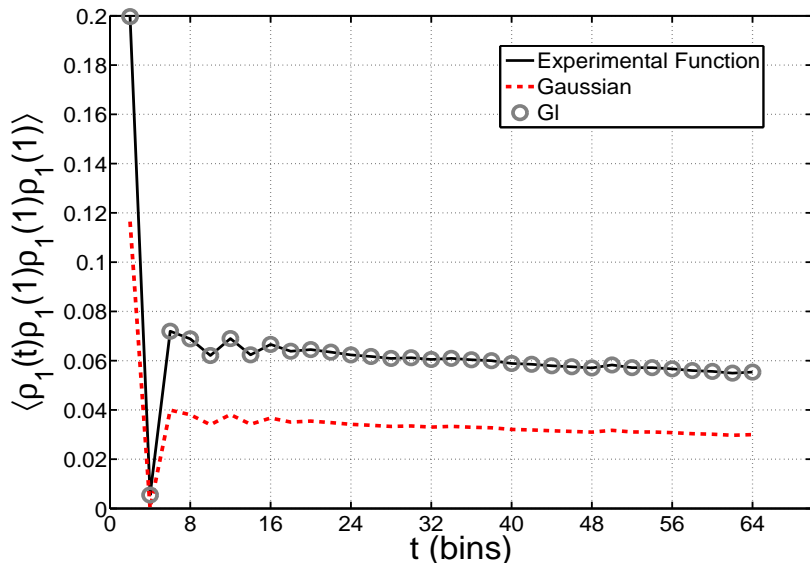


Figure 4: 4-point functions and its GI approximation. We plot  $R_{1111}(t_1, t_2 = t_3 = t_4 = 1)$  for window-size  $T_w = 64$  bins. The black continuous line is the experimental 4-point function. The dashed line is its Gaussian approximation without parametrization using equation 3.19. The circles represent its GI approximation 3.20.

In Figure 5 we show the GI approximation for the  $R_{1111}(t_1, t_2, t_3 = t_4 = 1)$  and its experimental version, which emphasizes the quality of the approximation. Using the same parameters for the other entries of  $R_{1111}$  and for  $R_{2222}$  results in a fitting error about 20 % larger.

One of the utilities of this representation will become apparent, once we deal with the solution of equation 2.15 in the next section.

## 4 A convenient set of functions to solve for second order kernels

---

At this point it is convenient to introduce a complete set of basis functions  $f_\mu(t), \mu = 1, 2, \dots, n_f$  to expand our variables in. We thus trade continuous time-arguments for discrete Greek indices. We expand our second order

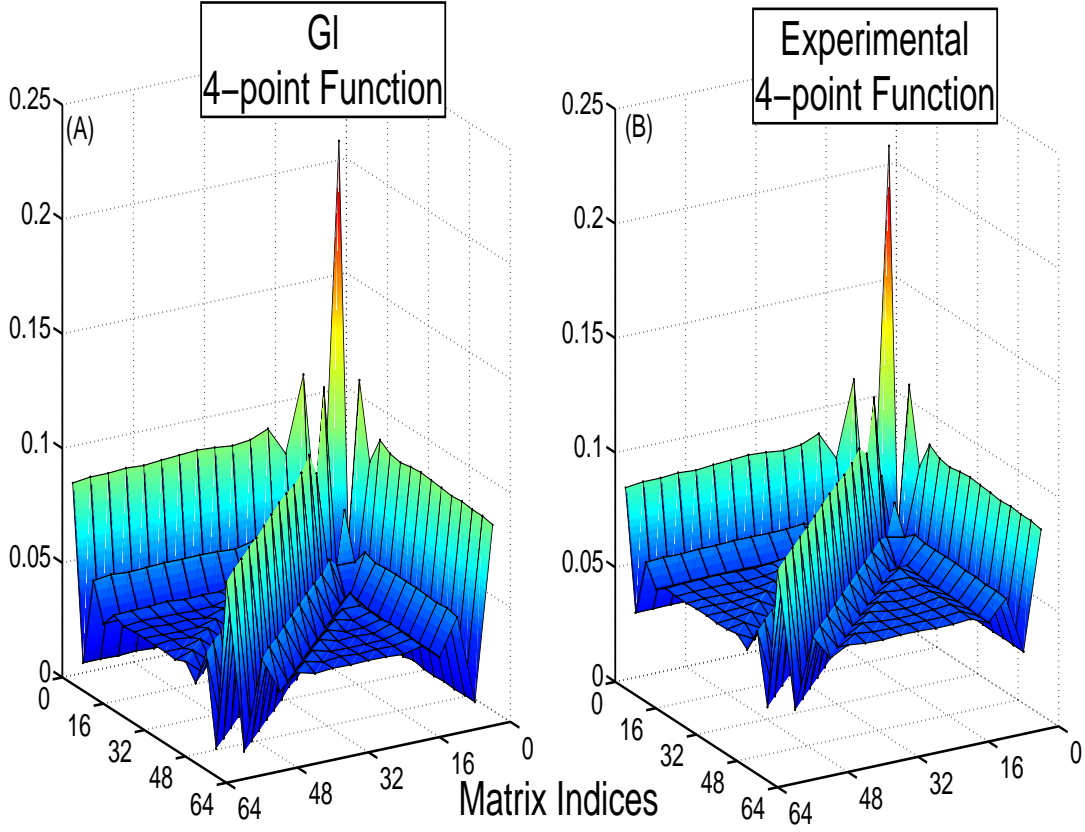


Figure 5: (A) GI approximation and (B) experimental 4-point function for  $R_{1111}(t_1, t_2, t_3 = t_4 = 1)$  for window-size  $T_w = 64$  bins.

kernels as:

$$K_{ab}(t_1, t_2) = \sum_{\mu, \nu} f_{\mu}(t_1) f_{\nu}(t_2) \mathcal{D}_{\mu\nu}^{ab}. \quad (4.22)$$

We also expand our correlation functions:

$$\mathcal{R}_{ab}^{(2)}(t_1, t_2) = \sum_{\mu, \nu} \mathcal{S}_{\mu\nu}^{ab} f_{\mu}(t_1) f_{\nu}(t_2) \quad (4.23)$$

and

$$R_{abcd}^{(4)}(t_1, t_2, t_3, t_4) =$$

$$\sum_{\alpha\beta\mu\nu} \mathcal{R}_{\alpha\beta\mu\nu}^{abcd} f_{\alpha}(t_1) f_{\beta}(t_2) f_{\mu}(t_3) f_{\nu}(t_4). \quad (4.24)$$

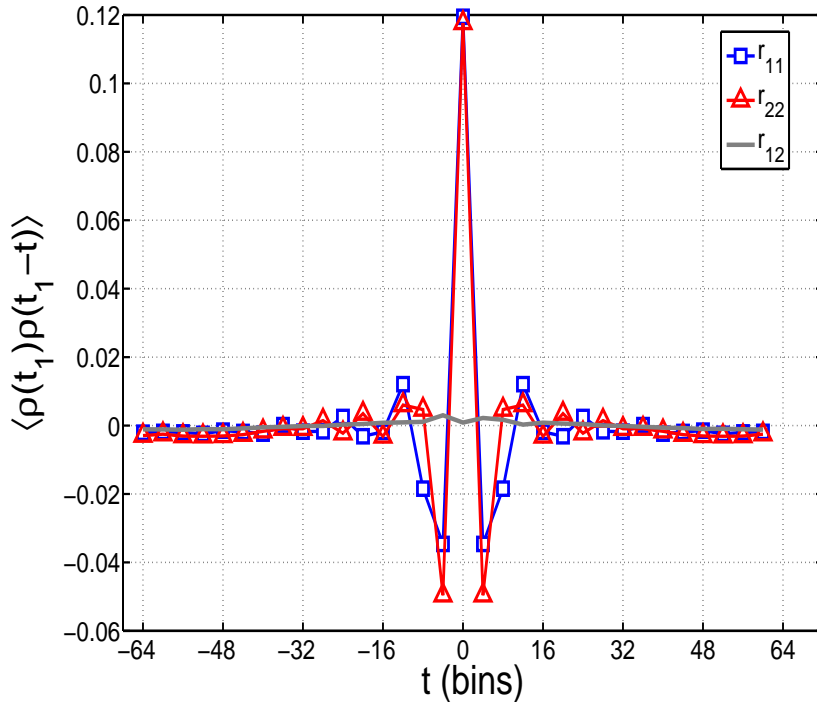


Figure 6: 2-point correlation functions  $r_{11}(t) = \langle \rho_1(t_1 - t) \rho_1(t_1) \rangle$ ,  $r_{22}(t) = \langle \rho_2(t_1 - t) \rho_2(t_1) \rangle$  and  $r_{12}(t) = \langle \rho_1(t_1 - t) \rho_2(t_1) \rangle$ . The central peak is absent in the mixed correlation function  $r_{12}(t)$ .

In order to efficiently compute our second order kernels it is crucial to select an adequate set for  $f_{\mu}(t)$ ,  $\mu = 1, 2, \dots, n_f$ .

Depending on the case, it may be sufficient to use a small number  $n_f$  of functions  $f_{\mu}(t)$  to get a useful representation. If  $n_f$  has only a slight dependence on window size  $T_w$ , this would allow one to increase  $T_w$  without further computational costs.

Often a Fourier expansion is used, i.e.  $f_{\omega} = e^{i\omega t}$ . But we may exploit our liberty to choose the functions in a more profitable way. Since our 2-point function  $R(t_1, t_2)$  is real, positive<sup>7</sup> and symmetric in  $t_1, t_2$ , it posses a

<sup>7</sup>In case this is not true, we just add a convenient constant.

complete set of eigenfunctions  $h_\mu(t)$ :

$$\int dt_2 R(t_1, t_2) h_\mu(t_2) = r_\mu h_\mu(t_1) \quad (4.25)$$

with eigenvalues  $r_\mu, \mu = 1, \dots, N_w$ . We now choose our functions as  $f_\mu(t) = h_\mu(t)/\sqrt{r_\mu}$ , which satisfy:

$$\int dt_1 dt_2 f_\mu(t_1) R(t_1, t_2) f_\nu(t_2) = \delta_{\mu\nu}. \quad (4.26)$$

This choice will avoid large matrix inversions, if at least part of our higher order correlation functions can be built from  $R(t_1, t_2)$ .

Substituting the expansions 4.23 and 4.24 into equations 2.15, we get a linear system to be solved for  $\mathcal{D}_{\mu\nu}^{ab}$ :

$$\mathcal{S}_{ab}^{\mu\nu} = \sum_{cd, \alpha\beta} \mathcal{R}_{abcd}^{\mu\nu\alpha\beta} \mathcal{D}_{cd}^{\alpha\beta} \quad (4.27)$$

In order to avoid cluttering our expressions with indices, we introduce our representation first for one neuron only, suppressing thus the indices  $a, b, \dots$ , all set to 1. We choose our functions  $f_\mu(t)$  to diagonalize  $R^{11}(t_1, t_2) = \langle \rho_1(t_1) \rho_2(t_2) \rangle$ :

$$\int dt_1 dt_2 f_\mu(t_1) R^{11}(t_1, t_2) f_\nu(t_2) = \delta_{\mu\nu}. \quad (4.28)$$

The first of equations 3.21 for  $\mathcal{R}_{\mu\nu\alpha\beta}^{1111}$  becomes

$$\mathcal{R}_{\mu\nu\alpha\beta} = A(\delta_{\mu\nu}\delta_{\alpha\beta} + 2\delta_{\mu\alpha}\delta_{\nu\beta}) - 2B n_\alpha n_\beta n_\mu n_\nu, \quad (4.29)$$

where  $n_\mu = \int dt f_\mu(t) \langle \rho(t) \rangle$ .

Using this expression and the shorthand  $\mathcal{S}_{\mu\nu} \equiv \mathcal{S}_{\mu\nu}^{11}$  in equations 4.27, we get the following equations for the unknown coefficients  $\mathcal{D}_{\mu\nu} \equiv \mathcal{D}_{\mu\nu}^{11}$

$$\mathcal{S}_{\mu\nu} = A[\text{tr}(\mathcal{D})\delta_{\mu\nu} + 2\mathcal{D}_{\mu\nu}] - 2B D_{nn} n_\nu n_\mu, \quad (4.30)$$

where  $\text{tr}(\mathcal{D}) \equiv \sum_\mu \mathcal{D}_{\mu\mu}$  and  $D_{nn} \equiv \sum_{\alpha\beta} n_\alpha \mathcal{D}_{\alpha\beta} n_\beta$ . The sums over  $\mu, \alpha, \beta$  run from 1 to  $T_w$  bins.

This system can now easily be solved by:

1. taking the trace over  $\mu\nu$  to compute  $\text{tr}(\mathcal{D}) \equiv D$  and

2. multiplying by  $n_\mu, n_\nu$  to compute  $D_{nn}$ .

We get

$$\mathcal{D}_{\mu\nu} = [\mathcal{S}_{\mu\nu}/A - D \delta_{\mu\nu} + 2Bn_\mu n_\nu D_{nn}]/2, \quad (4.31)$$

with

$$D = [2(1 - n_4)\mathcal{S}_{\mu\mu} + 2n_2 n_\mu \mathcal{S}_{\mu\nu} n_\nu]/\Delta, \quad (4.32)$$

$$D_{nn} = [(n + 2)n_\mu \mathcal{S}_{\mu\nu} n_\nu - \mathcal{S}_{\mu\mu} n_2]/\Delta, \quad (4.33)$$

where

$$\Delta = 2(T_w + 2)(1 - n_4) + 2n^2, n_2 \equiv \sum_{\mu} n_\mu n_\mu, n_4 \equiv (n_2)^2. \quad (4.34)$$

For two neurons we now have to decorate our formulas with the indices  $a, b, \dots$ . To simplify our formulas, we assume symmetry between the two neurons:  $R_{11} = R_{22}$ , which in our case is very well satisfied - see Figure 6.

The 4-point functions are now represented as

$$\begin{aligned} \mathcal{R}_{1111}^{\mu\nu\alpha\beta} &= [\delta_{\mu\nu}\delta_{\alpha\beta} + \delta_{\mu\alpha}\delta_{\nu\beta} + \delta_{\mu\beta}\delta_{\nu\alpha}]A_{1111} + B_{1111}^{\alpha\beta\mu\nu} \\ \mathcal{R}_{1112}^{\mu\nu\alpha\beta} &= [\delta_{\mu\nu}R_{12}^{\alpha\beta} + \delta_{\mu\alpha}R_{12}^{\nu\beta} + \delta_{\nu\alpha}R_{12}^{\mu\beta}]A_{1112} + B_{1112}^{\alpha\beta\mu\nu} \\ \mathcal{R}_{1122}^{\mu\nu\alpha\beta} &= [\delta_{\mu\nu}\delta_{\alpha\beta} + R_{12}^{\mu\alpha}R_{12}^{\nu\beta} + R_{12}^{\mu\beta}R_{12}^{\nu\alpha}]A_{1122} + B_{1122}^{\alpha\beta\mu\nu} \\ \mathcal{R}_{1222}^{\mu\nu\alpha\beta} &= [R_{12}^{\mu\nu}\delta_{\alpha\beta} + R_{12}^{\mu\alpha}\delta_{\nu\beta} + R_{12}^{\mu\beta}\delta_{\nu\alpha}]A_{1222} + B_{1222}^{\alpha\beta\mu\nu} \\ \mathcal{R}_{2222}^{\mu\nu\alpha\beta} &= [\delta_{\mu\nu}\delta_{\alpha\beta} + \delta_{\mu\alpha}\delta_{\nu\beta} + \delta_{\mu\beta}\delta_{\nu\alpha}]A_{2222} + B_{2222}^{\alpha\beta\mu\nu}. \end{aligned} \quad (4.35)$$

The intermediate steps 1 and 2 leading to equation 4.30 now increase, since we have to express several 4-point functions in terms of 2-point functions, not all of them being diagonal. In the particular case of the two H1 neurons though, we may further simplify this system, neglecting  $R_{12}$ . Its effect<sup>8</sup> is very small indeed, since for rotational stimuli the action of the two neurons is complementary: an exciting stimulus for one neuron is inhibiting for the other - see Figure 6. Although for translational stimuli both neurons fire nearly synchronously, the dominant peak near  $\tau = 0$  in  $R_{12}$  is absent, since synchrony is not exact. In the following we therefore neglect  $K_{12}$ . As can be seen in Figure 7,  $K_{12}$  is only  $\sim K_{22}/5$ . Since the contributions of  $K_{11}$  and  $K_{22}$  are already small,  $K_{12}$ 's 1 % effect can be safely neglected for both types of stimuli.

Our equations now decouple and we get two sets identical to equations 4.27, one for each neuron.

---

<sup>8</sup>The effect of  $R^{12}$  may be included perturbatively- see section 6.

## 5 Reconstructing the fly's stimulus and measuring its quality

---

To test the quality of our reconstructions, we use the data with  $\eta \sim 0.8$ ,  $\tau = 10$  milliseconds and  $\langle r \rangle \sim 80$  spikes  $\text{sec}^{-1}$ .

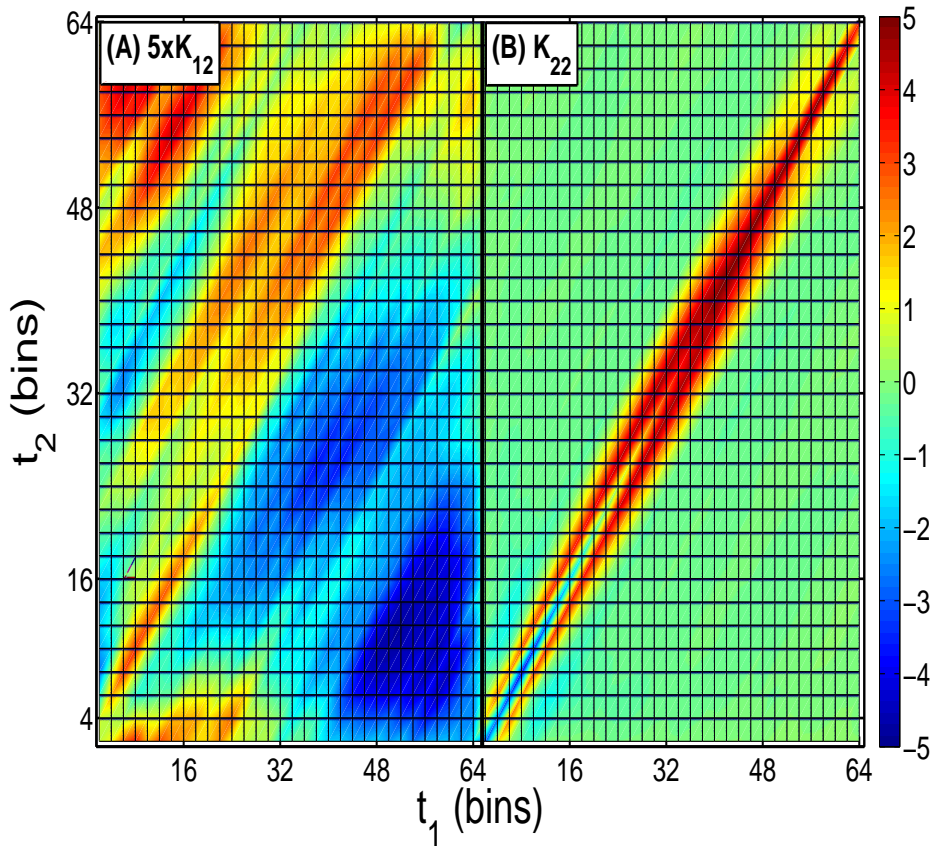


Figure 7: Second order kernel  $K_{22}(t_1, t_2)$  and upscaled version of  $K_{12}(t_1, t_2)$  for  $T_w = 64$ . (A)  $5 * K_{12}$ , (B)  $K_{22}$ . Notice  $K_{22}/K_{12} \sim 5$ .

We select a representative sample, one second long, of the experiment, in order to give a visual display of the reconstruction. In Figure 8 we show the first order reconstruction of the original stimulus using  $K_1$  and  $K_2$  and the second order reconstruction, where the effect of  $K_{11}$  and  $K_{22}$  is added - with

and without the GI-approximation. We conclude:

- Reconstructions using the experimental 4-point functions are very similar to their GI-approximation.
- The reconstruction procedure is unable to reproduce the fast stimulus variations at the 2 milliseconds time scale. It is also clear that still higher order terms are not going to improve this deficiency. But the second order kernels always represent an improvement, since the black line in Figure 8 is always a better approximation to the stimulus than the blue one.
- We observe a stimulus-to-spike delay time of  $t_{rot} \sim 20$  bins.

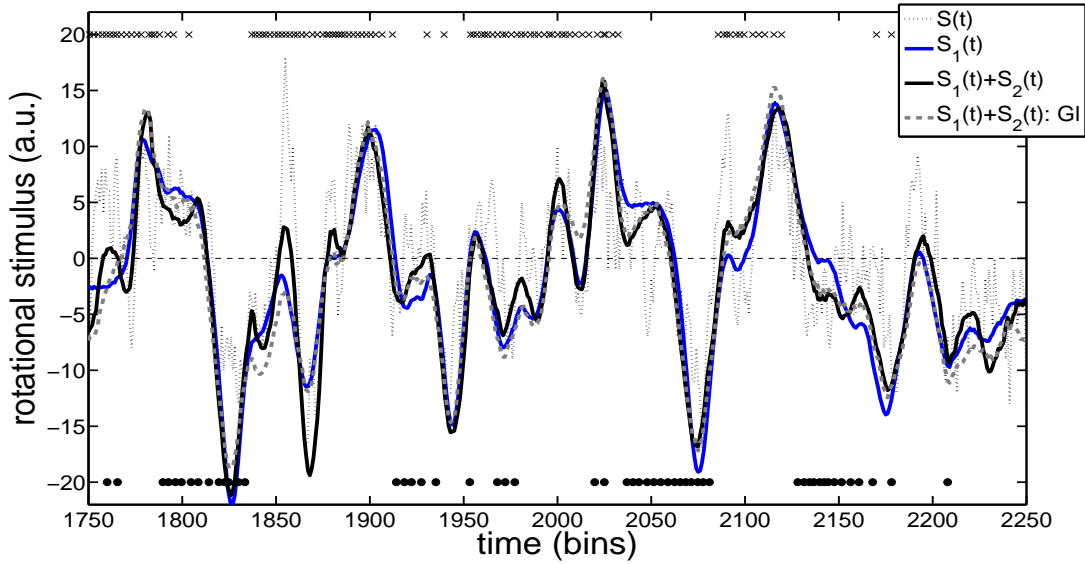


Figure 8: Reconstructing the rotational stimulus with kernels  $K_1$ ,  $K_2$  and  $K_{11}$ ,  $K_{22}$ , using the experimental 4-point function and the GI-approximation. Black thin dashed line:  $S(t)$ , input stimulus to be reconstructed, blue line:  $S_1(t)$ , reconstruction using only  $K_1$  and  $K_2$ , black continuous line:  $S_1(t) + S_2(t)$ , experimental second order reconstruction, gray dashed line:  $S_1(t) + S_2(t) : GI$ , GI-second order reconstruction. The  $\times$  and  $\bullet$  signs stand for the right and left spikes respectively. Observe a delay-time of about 20 bins.

Although visual appraisalment of the reconstruction quality is an indispensable guide to our intuition, numerical measures are less subjective. We naturally use the  $\chi^{(2)} = \langle \int dt [s_e(t) - s(t)]^2 \rangle$  of Equation 2.4, since its minimization was used to determine the kernels  $k_i, K_j$ . The reconstruction improvement due to second order kernel is reflected in

$$\delta\chi^{(2)} \equiv \frac{\chi_1^{(2)} - \chi_{12}^{(2)}}{\chi_1^{(2)}}, \quad (5.36)$$

where  $\chi_1^{(2)}$  takes only first order terms into account -  $\chi_1^{(2)} = \langle \int dt [s_1(t) - s(t)]^2 \rangle$ , whereas second order terms are included in  $\chi_{12}^{(2)} = \langle \int dt [s_1(t) + s_2(t) - s(t)]^2 \rangle$ .  $\delta\chi^{(2)}$  is positive, but small of  $\sim 8\%$ . The chi-squared difference between the experimental and GI-reconstructions is only of  $\sim 0.5\%$ .

Although the  $\chi^{(2)}$ -improvement is small, second order terms are a important at specific stimulus-dependent instants. In order to assess the relevance of these, we measure *local chi-squares*, defined as:

$$\chi_1^2(t, \Delta T) \equiv \int_{t-\Delta T}^{t+\Delta T} dt \langle (s_1(t) - s(t))^2 \rangle \quad (5.37)$$

and

$$\chi_{12}^2(t) \equiv \int_{t-\Delta T}^{t+\Delta T} dt \langle (s_1(t) + s_2(t) - s(t))^2 \rangle, \quad (5.38)$$

for  $t = T_2$ , where  $T_2$  are instants when  $\chi_{12}^2(t)$  is at least as important as  $\chi_1^2(t)$ . If  $N_2$  is the number of such windows of size  $\Delta T$  and  $N_T$  the duration of the experiment in bins divided by the window-size in bins, we plot in Figure 9 the fraction of the stimulus-dependent instants vs.  $\chi_1^2/\chi_{12}^2$ . Although this fraction vanishes as we require the importance of second order terms to increase, they still make a sizable contribution. Unfortunately just looking at the mean stimulus around  $T_2$  does not provide any insight and a more detailed analysis will be needed to reveal features, which might be relevant at these particular instants.

Here we only follow (Rieke et al., 1997) and separate systematic from random errors, decomposing the estimate  $\tilde{s}_e(\omega)$  into a frequency-dependent gain  $g(\omega)$  and an effective noise  $n_{eff}(\omega)$  referred to the input:

$$\tilde{s}_e(\omega) = g(\omega)[\tilde{s}(\omega) + n_{eff}(\omega)]. \quad (5.39)$$

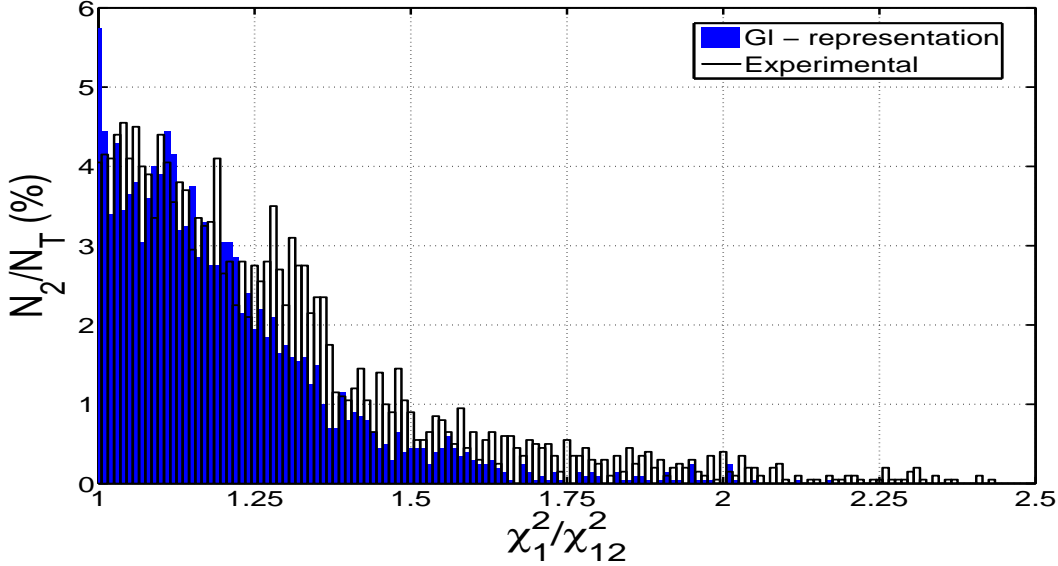


Figure 9:  $N_2/N_T$  versus  $\chi_1^2/\chi_{12}^2$  for experimental and GI-reconstruction. We find the instants where  $\chi_1^2/\chi_{12}^2$  assumes a particular value  $\geq 1$ , when computed in windows of size  $\Delta T = 64$  bins.  $N_2$  is the number of these windows, whereas  $N_T$  is the duration of the experiment in bins divided by the window size.

Around  $T_2$ , we observe an overall improvement of 20% in  $g(\omega)$ . A further indication, that second order contributions, although drowned in averages over the whole experiment, may nevertheless have crucial importance in improving the code at specific moments.

Finally we discuss the reconstruction of translational stimuli. Although in real life there is a continuous intermingling of *rotational* and *translational* motion, for a start we have considered this artificial separation of stimuli. Thus we have computed all averages  $\langle \cdot \rangle$  also for the translational setup. The kernels  $K_a, K_{ab}$  are similar to the rotational ones, but there is a sign change. Whereas for rotational stimuli  $K_1 \sim -K_2, K_{11} \sim -K_{22}$ , for the translational case we have

$$\begin{aligned} K_1^{(trans)} &\sim K_2^{(trans)} \sim K_1^{(rot)}, \\ K_{11}^{(trans)} &\sim K_{22}^{(trans)} \sim K_{11}^{(rot)}, \end{aligned} \quad (5.40)$$

The reconstructions shown in Figure 10 are worse than the rotational ones. For positive stimuli, corresponding to unrealistic backward motion of the

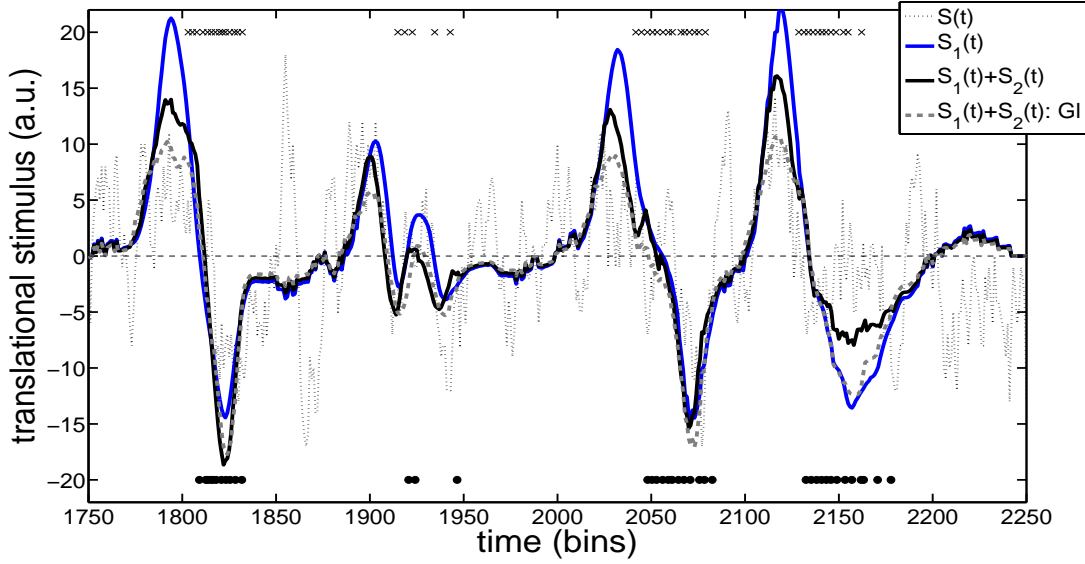


Figure 10: Reconstructing the translational stimulus with kernels  $K_1$ ,  $K_2$  and  $K_{11}$ ,  $K_{22}$ , using the experimental 4-point function and the GI-approximation. Black thin dashed line:  $S(t)$ , input stimulus to be reconstructed, blue line:  $S_1(t)$ , reconstruction using only  $K_1$  and  $K_2$ , black continuous line:  $S_1(t) + S_2(t)$ , experimental second order reconstruction, gray dashed line:  $S_1(t) + S_2(t) : GI$ , GI-second order reconstruction. The  $\times$  and  $\bullet$  signs stand for the right and left spikes respectively. Observe a delay-time of about 25 bins.

fly, both neurons fire vigorously, whereas in the opposite case none does. Interestingly, the delay-time is now  $t_{trans} \sim 25$  bins, about 5 bins larger than  $t_{rot}$ : inspite of their mutual inhibition, the neurons manage to fire, albeit a little bit retarded. The GI-representation works equally well for this case. It would be interesting to subject the fly to a more realistic mixture of rotational and translational motion without separating the two and then compute correlation functions etc. We intend to come back to this issue in the future.

## 6 Gl-approximation in population coding: taming the matrix explosion

---

Although the spike generation process of the H1 neurons is not Gaussian, the parametrization 3.20 is unexpectedly good. Actually we don't know how to judge from the spike interval distribution, whether this surprise will happen or not. In fact, the interval distribution of the spike times looks more nearly Poisson, instead of Gaussian. We remark, that independent increment probability distributions, whether they are Poisson or not, never do justice to correlated spike trains. On the other hand, if the 2-point function  $R(t)$  is to be a suitable building block to represent the 4-point function, then the parametrization, equation 3.20, is uniquely selected to be the most general one respecting the symmetry of  $R^{(4)}(1, 2, 3, 4)$ .

Since first order computations treat each neuron independently and do not take their mutual correlations into account, in the future one certainly would want to perform second order reconstructions to study the fly's visual system for more than two neurons. Our Gl-approximation makes these computations much more feasible. It should also work for correlation functions involving neurons not belonging to the fly's lobula plate.

In order to apply our Gl-approximation, we imposed the requirement  $R_{11} = R_{22}$  and we neglected  $R_{12}$ . This limitation may be relaxed in the following way<sup>9</sup>. One could set  $R_{12} = 0$  and use a different set of functions for each neuron, diagonalizing thus all 2-point functions  $\mathcal{R}_{aa}$  and compute the coefficients  $\mathcal{D}_{ab}$ . Then reexpand all variables in terms of one set of functions only and apply the procedure, which led to equation 4.31 for  $R_{12} \neq 0$ . If this does not lead to a closed set of equations, small effects may always be taken into account by a perturbative scheme to arbitrary order. In fact, suppose we have solved equation 4.27 for some representation of  $\mathcal{R}_{abcd}^{\mu\nu\alpha\beta}$  - e.g. as we did in section 3. Incorporating  $R_{12} \neq 0$  and/or  $R_{22}^{\mu\nu} \neq \delta_{\mu\nu}$  will change the  $\mathcal{R}$ -matrix into:

$$\mathcal{R}' = \mathcal{R} + \delta\mathcal{R}, \quad (6.41)$$

with  $\delta\mathcal{R}$  supposedly *small*. The new equations to be solved are:

$$\mathcal{S}_{ab}^{\mu\nu} = \sum_{cd, \alpha\beta} \mathcal{R}'_{abcd}{}^{\mu\nu\alpha\beta} \mathcal{D}'_{cd}{}^{\alpha\beta}, \quad (6.42)$$

---

<sup>9</sup>Here we only provided an outline, leaving a detailed analysis for a future publication.

where  $\mathcal{D}' = \mathcal{D} + \delta\mathcal{D}$  and  $\mathcal{D}$  satisfies the unprimed equations 4.27. Expanding both sides of equation 6.42 to first order in the corrections, we get the equations

$$-\sum_{cd,\alpha\beta} \delta\mathcal{R}_{abcd}^{\mu\nu\alpha\beta} \mathcal{D}_{cd}^{\alpha\beta} = \sum_{cd,\alpha\beta} \mathcal{R}_{abcd}^{\mu\nu\alpha\beta} \delta\mathcal{D}_{cd}^{\alpha\beta}, \quad (6.43)$$

to be solved for the unknowns  $\delta\mathcal{D}$ .  $(-\delta\mathcal{R} \cdot \mathcal{D})$  replaces the left-hand-side of equation 4.27 and couples the neurons. The right-hand-sides of the above equation and equation 4.27 have the same form and can therefore be solved in the same manner.

The GI-approximation could also be useful for other systems and this would be a considerable step forward in implementing coding involving a large population of neurons. One of the problems in second order reconstructions involving many neurons is the size-explosion of the 4-point function matrices alluded to at equation 2.18. If, e.g. we record from four neurons using 128 bin-sized windows, the length of the matrices to be inverted would be  $\sim 128^8 \times 2^8 \sim 10^{19}$ . With our approximation the size of the linear system to be solved grows only linearly with the number of neurons.

In order to use our approximation, one would have to check the window-size independence of the parameters  $A_{ab\dots}$  and  $B_{ab\dots}$  for some subset of the complete matrix-indices, to convince oneself of the adequacy of the approximation. Since in our case the matrices were still manageable, we could compute the experimental 4-point functions to verify this point, but this will in general not be possible.

## 7 Materials and Methods

---

Flies, immobilized with wax, viewed two Tektronix 608 Monitors M1, M2, one for each eye, from a distance of 12cm, as depicted in Figure 1. The monitors were horizontally centered, such that the mean spiking rates of the two neurons, averaged over several minutes, were equal. They were positioned, such that a straight line connecting the most sensitive spot of the compound eye to the monitor was perpendicular to the monitor's screen. The light intensity corresponds roughly to that seen by a fly at dusk (Steveninck, Lewen, Strong, Köberle, & Bialek, 1997). The stimulus was a rigidly moving vertical bar pattern with horizontal velocity  $v(t)$ . We discretise time in bins of 2 milliseconds, which is roughly the refractory period of the H1 neurons. The fly

therefore saw a new frame on the monitor every  $\delta t = 2$  milliseconds, whose change in position  $\delta x$  was given by  $\delta x(t) = v(t)\delta t$ .

The velocity  $v(t)$  was generated by an Ornstein-Uhlenbeck process with correlation times  $\tau_c = 0, 5$  and  $10$  ms<sup>10</sup>, i.e. the stimulus was taken from a Gaussian distribution with correlation function  $C(t) = e^{-t/\tau_c}$ . Experimental runs for each  $\tau_c$  lasted 45 minutes, consisting of 20 seconds long segments. In each segment, in the first 10 seconds the same stimulus was shown, whereas in the next 10 seconds the fly saw different stimuli.

## 8 Summary

---

The ability to reconstruct stimuli from the output of sensory neurons is a basic step in understanding how sensory systems operate. If intra- and inter-neuron correlations between the spikes emitted by neurons are to be taken into account, going beyond first order reconstructions is mandatory. In this case one has to face the size-explosion of higher order spike-spike correlation functions, the simplest being the 4-point correlation function necessary for a second order reconstruction. Our GI-representation of the 4-point function in terms of 2-point functions tames this problem. If this representation holds more generally, the coding in large populations would become more feasible.

For our case of the two H1 neurons of the fly, correlations between them may be neglected, since they are only of  $\sim 1$  %. We perform reconstructions using both the experimental and the GI-approximation for the 4-point functions involved. Both are very similar, their chi-squared differing by 0.5 %. To implement the GI-program for the two neurons, we found it convenient to expand our variables in terms of eigenfunctions of 2-point matrices. We propose a perturbative scheme in order to take the neglected correlations into account.

We find that second order terms always improve the reconstruction, although measured by a chi-squared averaged over the whole experiment this improvement is only at the 8% level. Yet these terms can represent a 100 % improvement at special instants as measured by an instant dependent chi-squared.

---

<sup>10</sup>Although we show results only for  $\tau_c = 10$  ms our conclusions are also valid for  $\tau_c = 0, 5$  ms.

## Acknowledgments

---

We thank I. Zuccoloto for her help with the experiments. The laboratory was partially funded by FAPESP grant 0203565-4. NMF and BDLP were supported by FAPESP fellowships. We thank Altera Corporation for their University program and Scilab for its excellent software.

## References

- Bialek, W., Rieke, F., Steveninck, R. R. van, & Warland, D. (1991). Reading a neural code. *Science*, *252*(5014), 1854-1857.
- Brenner, N., Strong, S., Köberle, R., Bialek, W., & Steveninck, R. de Ruyter van. (2000). Synergy in a neural code. *Neural Computation*, *12*, 1531-1552.
- Farrow, K., Haag, J., & Borst, A. (2003). Input organization of multifunctional motion-sensitive neurons in the blowfly. *Journal of Neuroscience*, *23*(30), 9805-9811.
- Haag, J., & Borst, A. (2001). Recurrent network interactions underlying flow-field selectivity of visual interneurons. *Journal of Neuroscience*, *21*(15), 5685-5692.
- Haag, J., & Borst, A. (2008). Electrical coupling of lobula plate tangential cells to a heterolateral motion-sensitive neuron in the fly. *Journal of Neuroscience*, *28*(53), 14435-14442.
- Haag, J., Vermeulen, A., & Borst, A. (1999). The intrinsic electrophysiological characteristics of fly lobula plate tangential cells: Iii. visual response properties. *Journal of Computational Neuroscience*, *7*(3), 213-234.
- Hausen, K. (1981). Monokulare und Binokulare Bewegungsauswertung in der Lobula Plate der Fliege. *Verh. Dtsch. Zool. Ges.*, 49-70.
- Hausen, K. (1982). Motion sensitive interneurons in the optomotor system of the fly .2. the horizontal cells - receptive-field organization and response characteristics. *Biological Cybernetics*, *46*(1), 67-79.
- Hausen, K. (1984). The lobula-complex of the fly: structure, function and significance in visual behaviour. In M. All (Ed.), *Photoreception and vision in invertebrates*. New York: Plenum.
- Krapp, H. (2009). Sensory integration: Neuronal adaptations for robust visual self-motion estimation. *Current Biology*, *19*(10), R413-R416.

- Martin, S. (2006). *The volterra and wiener theories of nonlinear systems*.  
New York: Krieger Publishing Co.
- Rieke, F., Warland, D., Steveninck, R. de Ruyter van, & Bialek, W. (1997).  
*Spikes -exploring the neural code*. Cambridge ,USA: MIT Press.
- Steveninck, R. R. de Ruyter van, Lewen, G., Strong, S., Köberle, R., &  
Bialek, W. (1997). Reproducibility and variability in neural spike  
trains. *Science*, *275*, 1805-1808.